INTERNATIONAL JOURNAL FOR NUMERICAL METHODS IN FLUIDS, VOL. 15, 579–593 (1992)

A SPLIT OPERATOR SCHEME FOR OCEAN WAVE SIMULATION

CHI WAI LI

Department of Civil and Structural Engineering, Hong Kong Polytechnic, Hong Kong

SUMMARY

A coupled discrete spectral model was developed for the prediction of ocean waves by solving the energy conservation equation of the two-dimensional wave spectrum. The model includes the dispersion correction terms in the governing equation to account for the dispersive effect due to the frequency-dependent velocities of waves. A split operator scheme is used to deal with the numerical problems arising from different terms of the governing equation. The advection terms are solved by the proven accurate minimax characteristics method to avoid excessive numerical damping or oscillations. The dispersion correction terms are solved by central differencing. The source and sink terms are solved by a quasi-second-order explicit scheme with limitation on energy growth per time step to allow the use of a large time step. The model was verified by ideal test cases and wave-hindcasting studies under typhoon conditions in the South China Sea near Hong Kong.

KEY WORDS Split operator scheme Method of characteristics Ocean waves Wave spectrum

INTRODUCTION

The wave energy spectra generated under a complex wind field such as the passage of a typhoon can be multidirectional and multinodal.[1,2] A wave prediction model based on the significant wave height and period concept is not appropriate for dealing with this condition, while a numerical model based on the solution of the energy conservation equation of the two-dimensional wave spectrum (radiative transfer equation) is frequently used.

Although the expressions for the source terms (wind input, non-linear transfer and white-capping dissipation) in the radiative transfer equation have been known for many years, solutions of the equation through explicit computation of these source terms are expensive, since the non-linear transfer term is a five-dimensional integral. Consequently, various engineering simplifications of the non-linear transfer are employed in most models to enhance the computational efficiency, with the other source terms tuned to reproduce the observed results.[3] In addition, scattering of the field data used in the calibration study of various models causes the expressions for the source functions prescribed in the models to be inconsistent. The result is that the radiative transfer equation solved by different models is different.

Recently, the WAMDI group[4] developed a wave model WAM which prescribes all the source functions explicitly to reproduce the physics. The non-linear transfer term is computed through discrete interaction operator parametrization, which is general and reasonably accurate. The model was verified by ample field data. However, the model suffers from a severe numerical stability constraint unless a special treatment of the high-frequency tail of the computed spectrum

0271–2091/92/170579–15$12.50

Received June 1991
Revised March 1992

is imposed. Also, the model cannot describe the swell propagation accurately, since upwind differencing is used in the approximation of the advection terms.

This work reports the development of an ocean wave model using a split operator scheme. The governing equation is modified to account for the dispersive effect due to frequency-dependent wave velocities. The non-linear source terms in the equation are computed by a quasi-second-order explicit finite difference scheme, the advection terms are computed accurately by the minimax characteristics method[5] and the dispersion correction terms are computed by central differencing. The cause of instability of the model is studied and remedial work is done to allow for a large integration time step. The model is then applied to two wave-hindcasting studies of the South China Sea under typhoon conditions during which field data are available.

MODEL FORMULATION

The equation employed for wave prediction represents the energy conservation of a wave component of frequency f and direction θ measured from a reference axis in shallow water:

$$\frac{\partial F}{\partial t}+\frac{\partial}{\partial x}(c_g\cos\theta\, F)+\frac{\partial}{\partial y}(c_g\sin\theta\, F)+\frac{\partial}{\partial\theta}\left[\frac{c_g}{c}\left(\sin\theta\frac{\partial c}{\partial x}-\cos\theta\frac{\partial c}{\partial y}\right)F\right]=S_{in}+S_{nl}+S_{ds}+S_{bf}, \quad (1)$$

where $F(f, \theta, x, y, t)$ is the spectral density of the wave component (f, θ) at co-ordinates (x, y) and time t, c_g denotes the group velocity and c denotes the phase velocity. The relations among group velocity c_g, phase velocity c, wave number k, angular frequency $\omega\,(=2\pi f)$ and water depth H are

$$c_g=0{\cdot}5\left(\frac{g}{k}\tanh(kH)\right)^{1/2}\left(1+\frac{2kH}{\sinh(2kH)}\right), \quad (2a)$$

$$\omega=[gk\,\tanh(kH)]^{1/2}, \quad (2b)$$

$$c=[(g/k)\,\tanh\,(kH)]^{1/2}. \quad (2c)$$

The source functions take account of several energy input and dissipation processes: wind input S_{in}, non-linear transfer S_{nl}, white-capping dissipation S_{ds} and bottom friction S_{bf}. The expression for wind input is[6]

$$S_{in}=\max\left[0,\ 0{\cdot}25\frac{\rho_a}{\rho_w}\left(28\frac{u_*}{c}\cos\theta-1\right)\right]\omega F, \quad (3)$$

where u_* is the friction velocity and $\rho_a(\rho_w)$ is the density of air (water). The white-capping dissipation is[7]

$$S_{ds}=-2{\cdot}36\times10^{-5}\,\tilde{\omega}\frac{k}{\tilde{k}}\left[\frac{\tilde{\alpha}}{\tilde{\alpha}_{PM}}\right]^2F, \quad (4)$$

where $\tilde{\omega}$ is the mean angular frequency, $\tilde{k}$ is the mean wave number and

$$\tilde{\alpha}=E\tilde{k}^2, \quad (5)$$

E being the total energy. The bottom friction dissipation is

$$S_{bf}=-\frac{0{\cdot}038}{g^2}\frac{\omega^2}{\sinh^2(kH)}F, \quad (6)$$

which is obtained empirically in the JONSWAP study.[8] The non-linear transfer term S_{nl} is approximated as[9]

$$S_{nl}(k_4)=\left[1+\frac{5{\cdot}5}{k_4H}\left(1-\frac{5k_4H}{6}\right)\exp\left(-\frac{5k_4H}{4}\right)\right]\left(\sum_{i=1,2}A_i\omega_4[n_1^i\,n_2^i(n_3^i+n_4^i)-n_3^i\,n_4^i(n_1^i+n_2^i)]\right), \tag{7}$$

where A_i are the coupling coefficients and the action densities $n_j^i=F(k_j)/\omega_j$, $j=1,2,3$, are evaluated at discrete wave numbers $k_j^i=T_j^i$, which are related to the reference wave number k_4 through fixed linear transformations T_j^i.

DISPERSION CORRECTION

Since the wave velocities are dependent on the frequency, an initial wave energy distribution will spread over a large area when it is propagated over a long distance. The traditional numerical scheme is unable to account for this effect since it treats the frequency band as a single frequency. The consequence is that an initial spatial distribution of wave energy will disintegrate into a number of similar distributions ('sprinkler' effect).

In one dimension the pure advection of the wave spectrum is given by

$$\frac{\partial F}{\partial t}+c_g\frac{\partial F}{\partial x}=0. \tag{8}$$

In numerical models the propagation of finite spectral bands is considered instead of single components. For an initial distribution of energy in the frequency band $(f_i+\Delta f/2, f_i-\Delta f/2)$ the solution for the average energy is given by

$$\bar{F}(f_i, x, t)=F(f_i, x-c_g t, 0). \tag{9}$$

However, the solution should take account of the velocity difference within the spectral band. Since the velocity range within this band is approximately $(c_g-0{\cdot}5\Delta c_g, c_g+0{\cdot}5\Delta c_g)$, where $\Delta c_g\approx c_g\,\Delta f/f$, the average energy should be given by

$$\bar{F}(f, x, t)=\frac{1}{\Delta f}\int_{f_i-\Delta f/2}^{f_i+\Delta f/2}F(f, x-c_g(f)t, 0)\,\mathrm{d}f. \tag{10}$$

Assuming a quadratic variation of energy in $[x-c_g(f_i+\Delta f)\,t, x-c_g(f_i-\Delta f)\,t]$, we use Simpson's rule to get

$$\begin{aligned}\bar{F}(f, x, t)\approx{}&F(f_i+\Delta f, x-c_g(f_i+\Delta f)t, 0)+4F(f_i, x-c_g(f_i)t, 0)\\&+F(f_i-\Delta f, x-c_g(f_i-\Delta f)t, 0).\end{aligned} \tag{11}$$

By Taylor's series expansion and assuming a constant energy distribution in the frequency direction within the frequency band,

$$\bar{F}(f_i, x, t)\approx F(f_i, x-c_g(f_i)t, 0)+\frac{\Delta c_g^2(f_i)t^2}{6}\frac{\partial^2}{\partial x^2}F(f_i, x-c_g(f_i)t, 0). \tag{12}$$

The last term can be considered as a diffusion term of coefficient $\Delta c_g^2(f_i)t/24$. Such correction is similar to that proposed by Booij and Holthuijsen.[10] In differential form the equation can be

written as

$$\frac{\partial F}{\partial t}+c_g\frac{\partial F}{\partial x}=D\frac{\partial^2 F}{\partial x^2}, \tag{13}$$

where $D=\Delta c_g^2\tau/24$ and $\tau=t$.

In the presence of an energy generation term S_g the magnitude of the dispersion coefficient should be decreased owing to the energy introduced to the solution at later instants. The amount of decrease is assumed to be linearly dependent on the newly introduced energy:

$$\tau^{n+1}=\tau^n\left(1-\frac{S_g^n\Delta t}{F^n+S_g^n\Delta t}\right)+\Delta t. \tag{14}$$

In two dimensions the correction is similarly given by

$$\frac{\partial F}{\partial t}+c_g\cos\theta\frac{\partial F}{\partial x}+c_g\sin\theta\frac{\partial F}{\partial y}=D_{xx}\frac{\partial^2 F}{\partial x^2}+D_{yy}\frac{\partial^2 F}{\partial y^2}+2D_{xy}\frac{\partial^2 F}{\partial x\partial y}, \tag{15}$$

where

$$D_{xx}=D_{ss}\cos^2\theta+D_{nn}\sin^2\theta,\qquad D_{yy}=D_{ss}\sin^2\theta+D_{nn}\cos^2\theta\quad\text{and}\quad D_{xy}=(D_{ss}-D_{nn})\sin\theta\cos\theta,$$

with $D_{ss}=(\Delta c_g)^2\tau/24$ and $D_{nn}=c_g^2(\Delta\theta)^2\tau/24$; Δf and $\Delta\theta$ are the frequency and angular resolutions.

Including the dispersion correction terms, the energy conservation equation for the wave spectrum becomes

$$\frac{\partial F}{\partial t}+\frac{\partial}{\partial x}(c_g\cos\theta\,F)+\frac{\partial}{\partial y}(c_g\sin\theta\,F)+\frac{\partial}{\partial\theta}\left[\frac{c_g}{c}\left(\sin\theta\frac{\partial c}{\partial x}-\cos\theta\frac{\partial c}{\partial y}\right)F\right]$$
$$=S_{in}+S_{nl}+S_{ds}+S_{bf}+D_{xx}\frac{\partial^2 F}{\partial x^2}+D_{yy}\frac{\partial^2 F}{\partial y^2}+2D_{xy}\frac{\partial^2 F}{\partial x\partial y}. \tag{16}$$

NUMERICAL SCHEME

The split operator scheme (see e.g. Reference 11) is used in the numerical model. The solution to the governing equation at each time step is split into the following three fractional steps.

Advection step

$$\frac{F^{n+1/3}-F^n}{\Delta t}+c_g\cos\theta\frac{\partial F}{\partial x}+c_g\sin\theta\frac{\partial F}{\partial y}+\frac{c_g}{c}\left(\sin\theta\frac{\partial c}{\partial x}-\cos\theta\frac{\partial c}{\partial y}\right)\frac{\partial F}{\partial\theta}=0. \tag{17}$$

The equation simply states that the spectral density F is invariant along a ray under the effect of advection, refraction and shoaling. The solution is given by $F_{hijk}^{n+1/3}=F_{hi'j'k'}^n$, where $F_{hijk}^{n+1/3}=F(f_h,\theta_i,x_j,y_k,t_{n+1})$ represents the spectral density of frequency f_h and direction θ_i at time $t_n+\Delta t$ and position (x_j,y_k). The frequency f_h is constant along a ray. The position $(x_{j'},y_{k'})$ and direction $\theta_{i'}$ are determined by locating the ray path backwards in time according to the characteristic equations

$$\frac{dx}{dt}=c_g\cos\theta, \tag{18a}$$

$$\frac{dy}{dt}=c_g\sin\theta, \tag{18b}$$

$$\frac{d\theta}{dt}=\frac{\partial\theta}{\partial x}\frac{dx}{dt}+\frac{\partial\theta}{\partial y}\frac{dy}{dt}, \tag{18c}$$

$$\frac{dk}{dt}=\frac{\partial k}{\partial x}\frac{dx}{dt}+\frac{\partial k}{\partial y}\frac{dy}{dt}. \tag{18d}$$

Using Snell's law, which is expressed as

$$\frac{\partial}{\partial x}(k\sin\theta)-\frac{\partial}{\partial y}(k\cos\theta)=0, \tag{19}$$

and, from equation (2b),

$$\delta\omega=\frac{\partial\omega}{\partial H}\delta H+\frac{\partial\omega}{\partial k}\delta k=0, \tag{20}$$

equations (18c) and (18d) can be transformed to

$$\frac{d\theta}{dt}=\frac{1}{k}\frac{\partial\omega}{\partial H}\left(\sin\theta\frac{\partial H}{\partial x}-\cos\theta\frac{\partial H}{\partial y}\right), \tag{21a}$$

$$\frac{dk}{dt}=-\frac{\partial\omega}{\partial H}\left(\cos\theta\frac{\partial H}{\partial x}+\sin\theta\frac{\partial H}{\partial y}\right). \tag{21b}$$

The value $F^n_{ii'j'k'}$ is obtained by the minimax characteristics method,[5] which is a backward characteristics method with quadratic interpolation derived from a minimax criterion. This interpolation scheme is unconditionally stable, reasonably accurate and relatively efficient. The interpolation covers 4×4 nodes in space and four angles in direction. The scheme can be written as

$$F^{n+1/3}_{ijk}=\sum_{r=1}^{4}\phi_r(\gamma)\left[\sum_{p=1}^{4}\sum_{q=1}^{4}\phi_p(\alpha)\,\phi_q(\beta)\,F^n_{i'+r-3,\,j'+p-3,k'+q-3}\right], \tag{22}$$

where $\phi_1(\alpha)=\phi_4(\alpha)=-0{\cdot}25\alpha(1-\alpha)$, $\phi_2(\alpha)=1{\cdot}25\alpha-0{\cdot}25\alpha^2$, $\phi_3(\alpha)=1-0{\cdot}75\alpha-0{\cdot}25\alpha^2$ and α, β and γ are the interpolation parameters directions in x, y and θ respectively. In most cases the depth variation is small, so that $\gamma\approx0$ and the interpolation computation in θ can be bypassed. An illustration of the method in two dimensions is shown in Figure 1.

Dispersion correction step

$$\frac{F^{n+2/3}-F^{n+1/3}}{\Delta t}=D_{xx}\frac{\partial^2F}{\partial x^2}+D_{yy}\frac{\partial^2F}{\partial y^2}+2D_{xy}\frac{\partial^2F}{\partial x\partial y}. \tag{23}$$

The standard forward time, centred space scheme[12] is used in the solution. The stability limit is

$$\Delta t\leqslant\frac{1}{2}\left[\frac{D_{xx}}{\Delta x^2}+\frac{D_{xy}}{2\Delta x\Delta y}+\frac{D_{yy}}{\Delta y^2}\right]^{-1}. \tag{24}$$

Source input step

$$\begin{aligned}\frac{F^{n+1}-F^{n+2/3}}{\Delta t}&=S_{\text{in}}+S_{\text{nl}}+S_{\text{ds}}+S_{\text{bf}}-\left\{\frac{\partial}{\partial x}(c_g\cos\theta)+\frac{\partial}{\partial y}(c_g\sin\theta)\right.\\&\left.+\frac{\partial}{\partial\theta}\left[\frac{c_g}{c}\left(\sin\theta\frac{\partial c}{\partial x}-\cos\theta\frac{\partial c}{\partial y}\right)\right]\right\}F\\&=S_{\text{nl}}+\lambda F.\end{aligned} \tag{25}$$

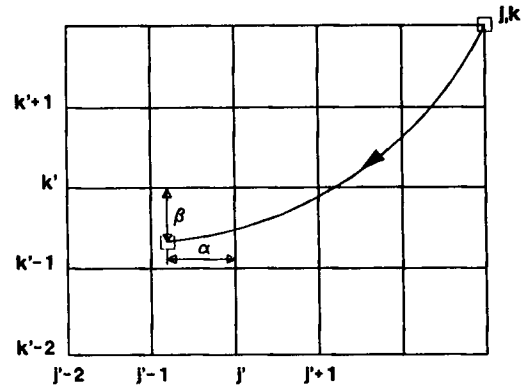

Figure 1. Illustration of the minimax characteristics in two dimensions

The coefficient of the refraction and shoaling terms of the above equation can be precomputed and stored to enhance the computational efficiency. A quasi-second-order explicit scheme which treats the non-linear transfer by the Euler scheme and the other sources by the Lax–Wendroff scheme (denoted as E–LW) is chosen in the source integration step to enhance the computational efficiency and accuracy:

$$F^{n+1} = F^{n+2/3} + \Delta t\,(\lambda^{n+2/3} F^{n+2/3} + S_{\mathrm{nl}}^{n+2/3}) + \frac{\Delta t^2}{2}(\lambda^{n+2/3})^2 F^{n+2/3}. \tag{26}$$

In the case where large time step is used (larger than 2 min in the numerical experiments), it was found that the scheme is unstable owing to the non-linear transfer terms. A restriction on the growth of energy per time step is imposed to enhance the stability and to allow the use of a large time step (15–20 min); empirically,

$$\Delta F < 0{\cdot}1\,[\alpha g^2/(2\pi)^4]/f^5 \tag{27}$$

where ΔF is the increase in energy per time step and $[\alpha g^2/(2\pi)^4]/f^5$ is a rough estimate of the highest spectral level to be reached. In the subsequent test it is demonstrated that such an imposition on wave growth only marginally affects the results.

MODEL VERIFICATION

Swell propagation

To study the performance of the scheme under pure advection, we consider the propagation of a swell in a horizontal plane of area 1500×1500 km^2 (roughly the dimensions of the South China Sea) covered with a grid of 50×50 km^2 mesh size. The time step chosen in the numerical computation is 0·5 h and the period of propagation is 24 h. The initial distribution of wave energy is Gaussian, with a standard deviation of 75 km, centred at location (300 km, 300 km) (Figure 2(a)). The spectrum at each spatial point is of Pierson–Moskowitz (PM) type with a $\cos^2\theta$

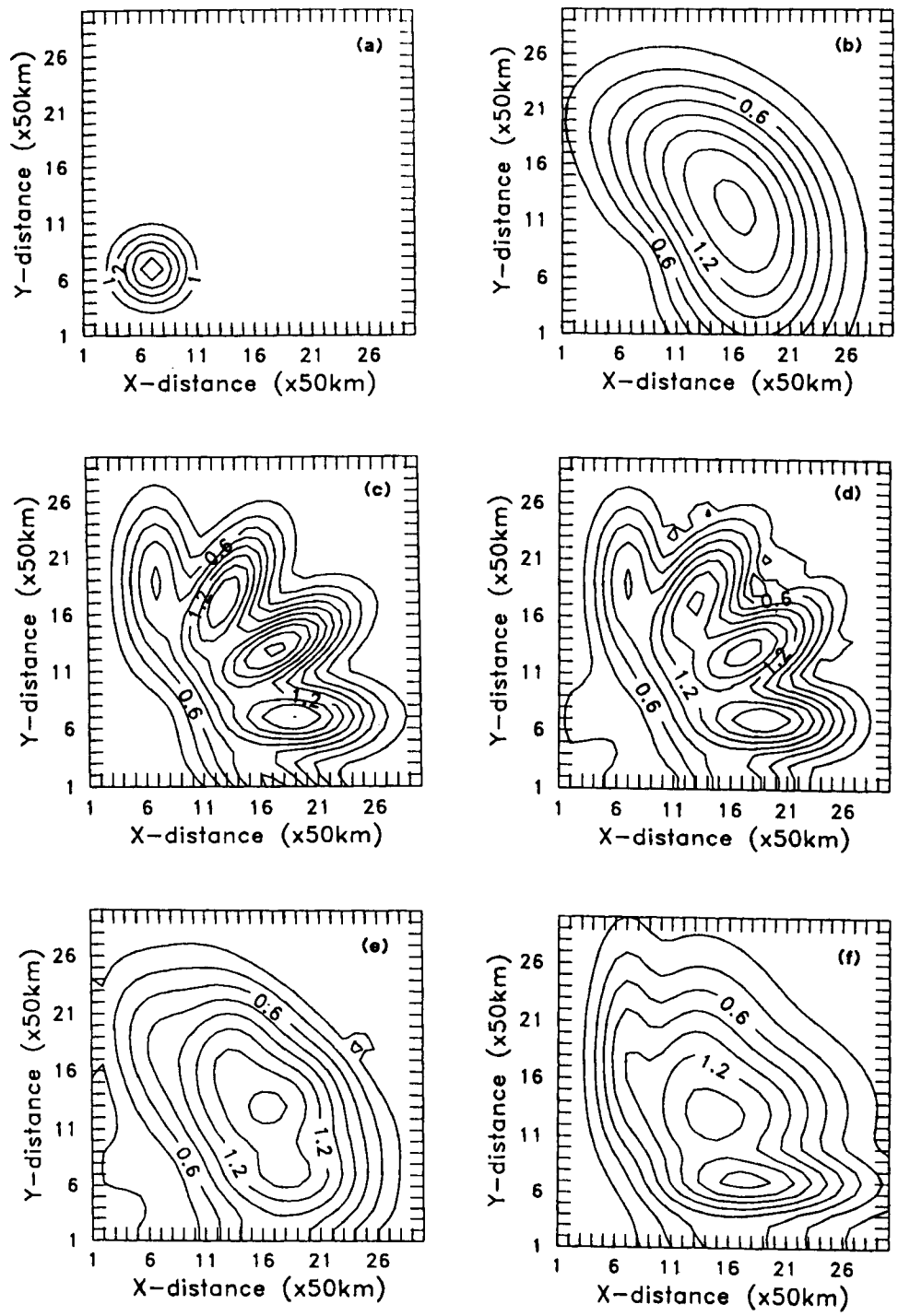

Figure 2. Modelling of swell propagation: (a) initial condition; (b) exact solution; (c) analytic solution on coarse grid; (d) solution by minimax characteristics method; (e) solution by minimax characteristics method with dispersion correction; (f) solution by upwind difference

directional distribution:

$$F(f,\theta,x,y,0)=\frac{2}{\pi}g^2(2\pi)^{-4}f^{-5}\exp\left[-1{\cdot}25\left(\frac{f}{f_p}\right)^{-4}\right]\cos^2(\theta-\theta_0)\alpha\exp\left(-\frac{(x-x_0)^2}{2\sigma_x^2}-\frac{(y-y_0)^2}{2\sigma_y^2}\right). \tag{28}$$

The peak frequency $f_p=0{\cdot}1$ Hz, $\alpha=0{\cdot}0016$, $x_0=300$ km, $y_0=300$ km and $\theta_0=0°$.

The nearly exact solution of the spatial distribution of the significant wave height for the wave spectrum is shown in Figure 2(b), which is obtained from the characteristic equation

$$F(f,\theta,x,y,t)=F(f,\theta,x-c_g\cos\theta\, t,\, y-c_g\sin\theta\, t,\, 0), \tag{29}$$

and the solution is computed with a high spectral resolution of 25 frequency bands, spanning the frequency range from 0·04 to 0·4 Hz, and 72 directional bands, with 5° resolution. In contrast, Figure 2(c) displays the analytic solution with a coarse spectral resolution of 25 frequency bands (same as the previous case) and 12 directional bands (30° resolution). Such a spectral resolution is frequently used in operational wave models. From the solution it can be seen that the 'sprinkler effect' is apparent. Figure 2(d) displays the corresponding solution using the minimax characteristics method. The 'sprinkler effect' is reproduced owing to the high accuracy of the scheme. On adding the dispersion correction to account for the spreading of the spatial wave energy distribution (Figure 2(e)), the solution is close to the exact solution. In addition, the result of using the upwind difference scheme, which introduces large numerical diffusion, is shown in Figure 2(f).

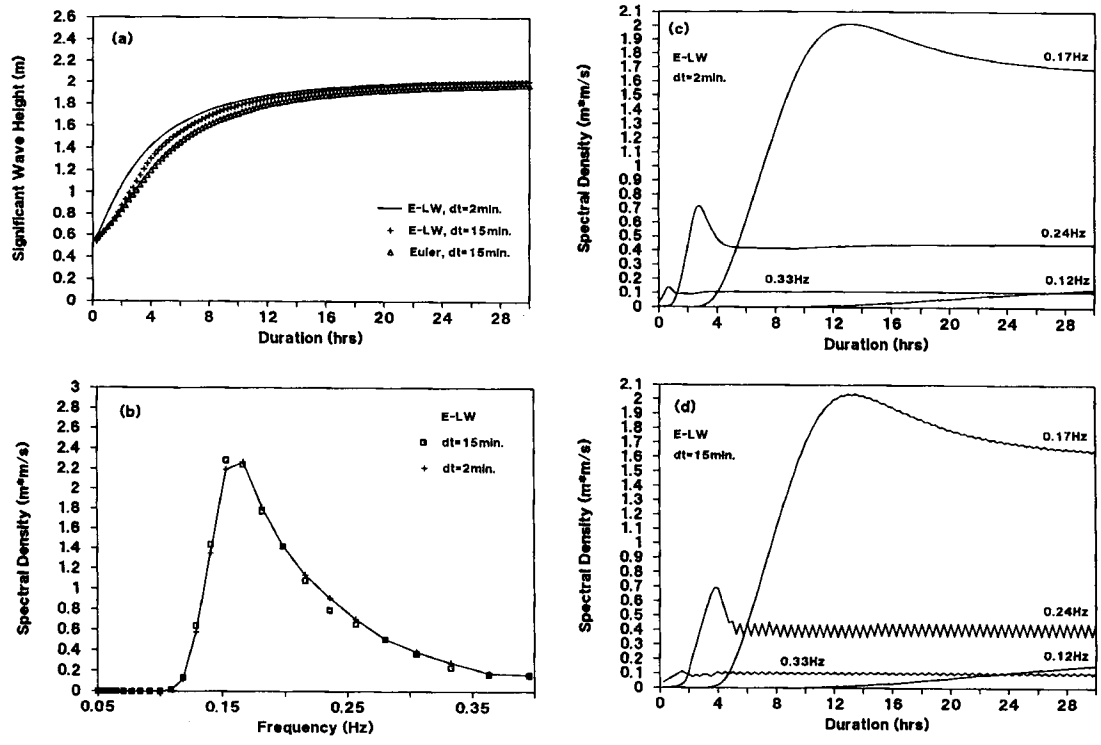

Figure 3. Duration-limited growth of waves: (a) significant wave height; (b) 1D spectra; (c), (d) time histories of typical wave components

Although the scheme accounts partly for the spreading of the spatial wave energy distribution and produces an acceptable solution, the numerical diffusion is anisotropic and cannot be adjusted to improve the accuracy if the time step and grid size are fixed.

Duration-limited growth of waves

The case of wave growth under a constant wind speed over an infinite region is considered to examine the performance of the source approximation. The stability constraint of the source integration scheme is not known owing to the non-linear nature of the non-linear energy transfer and the white-capping dissipation. In the subsequent test of the model it was found that a very small time step (1–2 min) is needed to avoid instability. The numerical instability occurs at the high-frequency tail, where the energy growth per time step is large compared with the magnitude of the spectral components. Since the practical time step size for prototype simulation is of the order of 10 min, a special treatment of the high-frequency tail of the spectrum to allow the use of a large time step is essential. The treatment is that a restriction on the growth of the spectrum per time step is included in the model such that the maximum increase per time step is less than a certain value, equation (27). The justification for imposing such a restriction is that we are not interested in the solution of the high-frequency region, since most energy is in the low-frequency region.

After implementation of the above restriction in the model the maximum allowable time step can be increased to about 15–20 min and the accuracy is still acceptable. Figure 3(a) displays the computed significant wave height of duration-limited wave growth under a wind speed of $10\,m\,s^{-1}$ using 2 and 15 min time steps by the E–LW scheme. The maximum difference in the

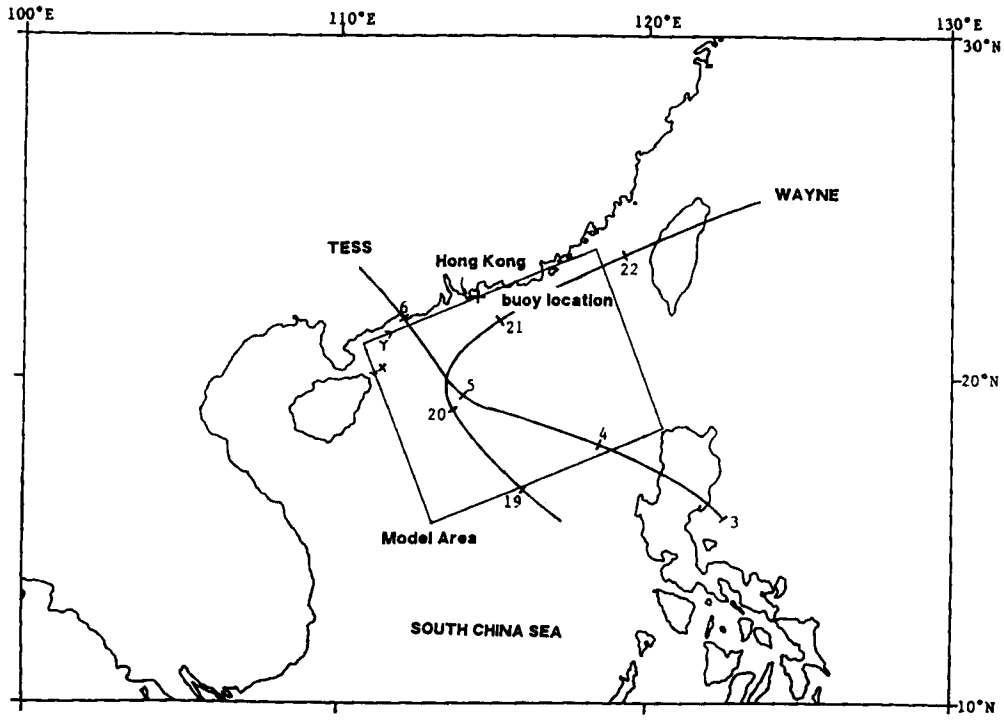

Figure 4. Model simulation area and tracks of typhoons

resulting non-dimensional energies is only 10%. The inferior performance incurred by using the first-order Euler scheme in the source integration is also displayed. In addition, the difference in the computed one-dimensional spectra for the two cases is small (Figure 3(b)) and the restriction only affected the wave components slightly (Figures 3(c) and 3(d)). In the commonly encountered range of wind speed (about 0–30 m s^{-1}) the above restriction was found to affect the results only slightly provided that the time step used was not too large (around 10 min).

Typhoon-generated waves in the South China Sea near Hong Kong

The model was evaluated against the field data collected in the wave measurement programme in the South China Sea near Hong Kong under typhoon conditions in 1985–1986.[13] Four series of measurements were carried out within this period. Raw data of surface elevation were recorded by a Waverider buoy for several days during the passage of typhoons. For brevity, only the results of simulation during two typhoons are displayed.

The computational grid chosen in the simulation and the location of the measurement site are shown in Figure 4. One boundary of the grid is in alignment with the coastline to minimize the numerical error introduced at the boundary. The grid size is 50×50 km^2. The time integration step is 15 min. We chose 25 frequency bands on a logarithmic scale, with $\Delta f/f = 0{\cdot}09$, spanning a frequency range $f_{max}/f_{min} = 7{\cdot}9$, and 12 directional bands (30° resolution). The frequency interval extended from 0·05 to 0·40 Hz. The use of such an unequal frequency band has the advantages that there is a higher resolution in the low-frequency region and the computation of the non-linear transfer is more efficient.

The initial condition chosen in the model was a JONSWAP spectrum[8] with parameters $\alpha = 0{\cdot}018$, $\gamma = 3{\cdot}3$, $f_p = 0{\cdot}35$ Hz and $\sigma_a = \sigma_b = 0{\cdot}08$ and a directional distribution of the Mitsuyasu–Hasselmann form. A non-zero initial condition is essential in the model to trigger the growth of waves. At the outflow boundary no boundary condition is required. At the inflow boundary the boundary condition will depend on the wave condition outside the computational domain. At the water–land boundary a zero spectral value is imposed. At the water–water boundary a zero gradient is imposed, which is realistic if the wave condition is rather uniform spatially near the boundary.

Typhoon Tess appeared in September 1985 and typhoon Wayne in August 1986. The tracks of the two typhoons are shown in Figure 4 and the measurement site has a water depth 25 m. The marks on the typhoon tracks denote the beginning of each day and the numbers adjacent give the corresponding date. The wind input to the model is obtained from a model due to Jelesnianski[14]. The data needed for the wind field calculation are available at 6 h intervals. Linear interpolation is used to produce the data at 15 min intervals, which is compatible with the time step used in the wave model.

For typhoon Tess the measured and modelled significant wave heights at the site are shown in Figure 5(a). The agreement is on the whole satisfactory. At the wave growth stage the computed wave is higher than the measured wave; this is mainly due to the fact that the modelled wind speed is greater than the measured one (Figure 5(b)). The peak sea state persisted for a relatively long period in the field, even though the wind speed was decreasing. This may be caused by the propagation of swells from other areas. The computed averaged wave period displays a similar trend to that measured (Figure 5(c)) but with a consistently smaller value, indicating that the simulation time is not long enough for the energy transferring to the longer period.

Figures 6(a)–6(c) compare the measured and hindcast one-dimensional frequency spectra at different instants. The field data were sampled at a time interval of 0·39 s and each record lasted for 20 min. The field spectra are of frequency resolution 0·0025 Hz and were obtained by splitting

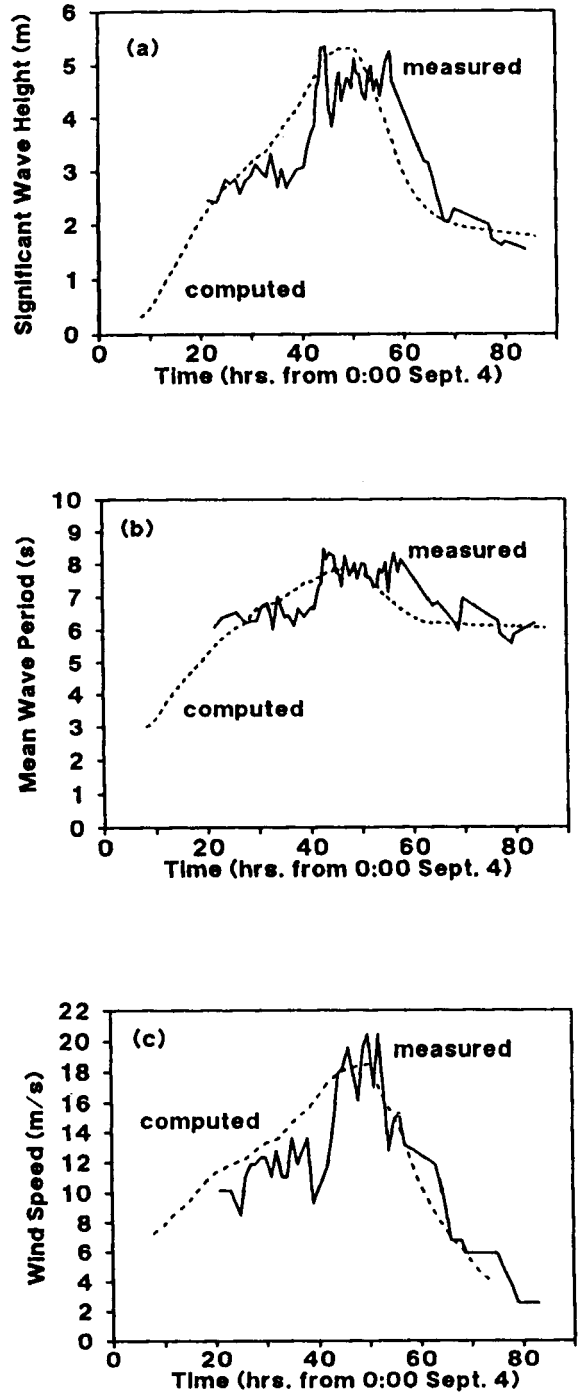

Figure 5. Wind wave simulation during typhoon Tess: (a) significant wave height; (b) average wave period; (c) wind speed

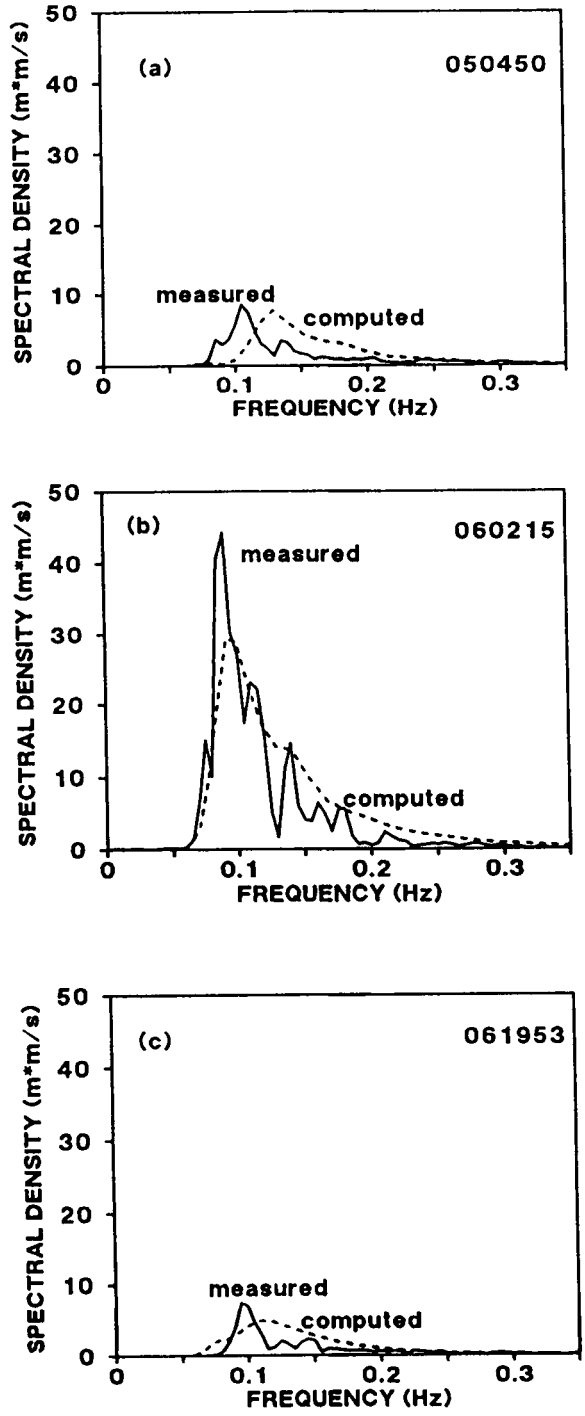

Figure 6. Spectra of typhoon Tess at various instants

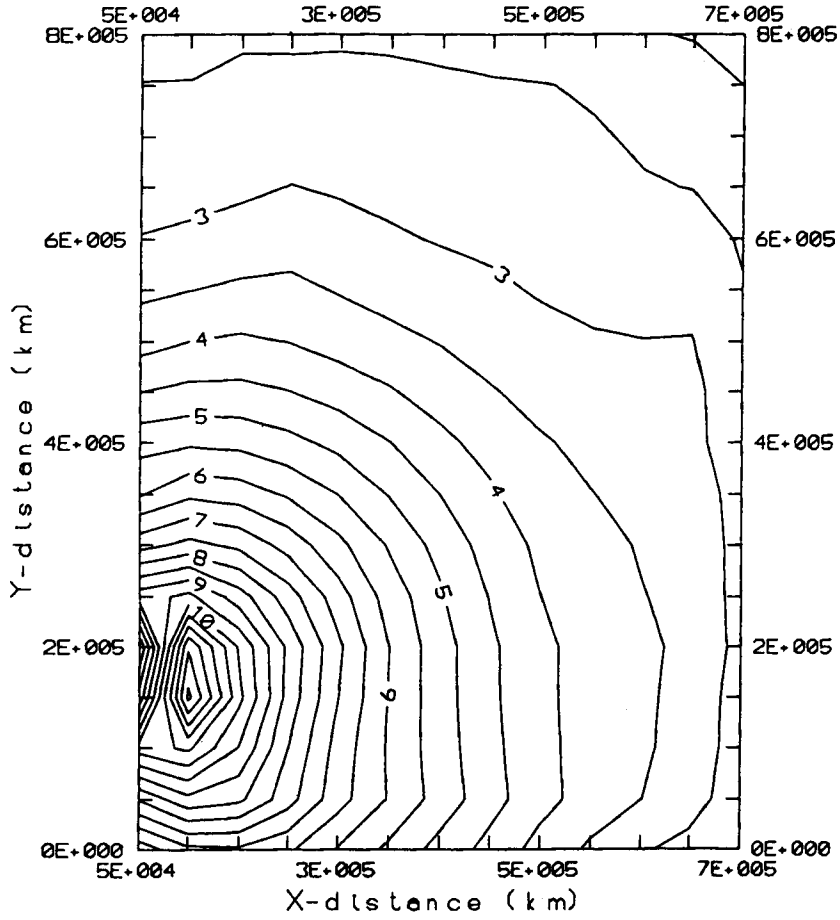

Figure 7. Typical spatial distribution of significant wave height during typhoon Tess

the record into six sections for averaging, a balance between resolution and reliability. The results show that the spectral shape and peak frequency are modelled correctly at the peak condition, whereas for the other instants the agreement is not so good.

The spatial distribution of significant wave height under the peak sea condition at Hong Kong is shown in Figure 7. The distribution on the whole follows the spatial distribution of the wind field. However, since no additional wind and wave data at other sites are available, verification of the model with respect to spatial prediction cannot be carried out.

For typhoon Wayne, Figure 8(a) compares the significant wave heights obtained by the model and at the measurement site. The hindcast sea state is lower than the measured one because the sea state in the model has insufficient time to build up and there may be the presence of distant swell. After 40 h the waves start to growth and reach a peak value about 0·5 m lower than that measured. The rate of decay of the waves is similar in both cases and hence the computed wave height is consistently lower than the measured wave height. Similar results are obtained for the averaged period (Figure 8(b)).

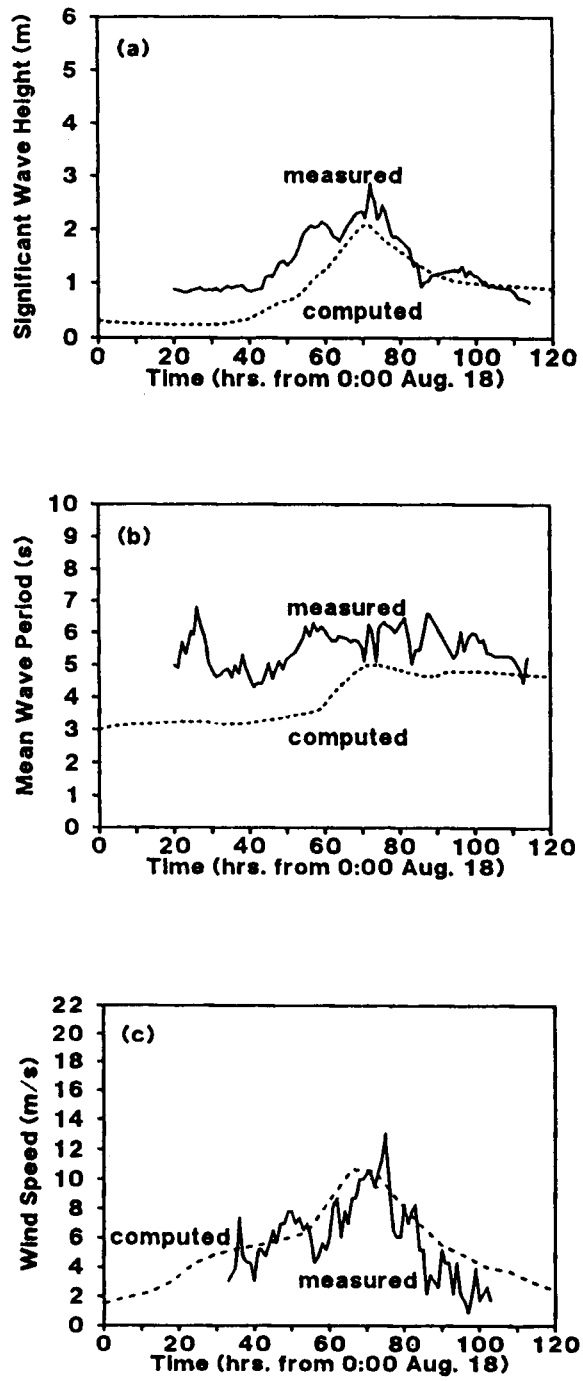

Figure 8. Wind wave simulation during typhoon Wayne: (a) significant wave height; (b) average wave period; (c) wind speed

CONCLUSIONS

A numerical model using a split operator algorithm was developed for ocean wave simulation. The use of the minimax characteristics method in the advection terms together with the inclusion of dispersion correction terms produces an accurate solution for swell propagation. The use of a quasi-second-order explicit scheme for the source terms together with a restriction of the energy growth per time step allows the use of a large time step. The results obtained from application of the model to the South China Sea under typhoon conditions are satisfactory.

ACKNOWLEDGEMENTS

This study is supported by a grant from the Hong Kong Polytechnic. Assistance from Mr. M. Mao is sincerely acknowledged.

REFERENCES

1. D. L. Harris, 'Models for the hurricane wave field', in *Wave Dynamics and Radio Probing of the Ocean Surface*, Plenum, New York, 1986, pp. 677–682.
2. CERC, *Shore Protection Manual*, Vol. 1, Department of the Army, U.S. Army Corps of Engineers, 1984.
3. The SWAMP group, 'Sea Wave Modelling Project (SWAMP). An intercomparison study of wind wave prediction models. Part 1: Principal results and conclusions', in *Ocean Wave Modelling*, Plenum, New York, 1985, pp. 1–256.
4. The WAMDI group, 'The WAM model—a third generation ocean wave prediction model', *J. Phys. Oceanogr.*, **18**, 1775–1810 (1988).
5. C. W. Li, 'Advection simulation by minimax-characteristics method', *J. Hydraul. Eng., ASCE*, **116**, 1138–1144 (1990).
6. R. L. Snyder *et al.*, 'Array measurements of atmospheric pressure fluctuations above surface gravity waves', *J. Fluid Mech.*, **102**, 1–59 (1981).
7. G. J. Komen *et al.*, 'On the existence of a fully developed wind-sea spectrum', *J. Phys. Oceanogr.*, **14**, 1271–1285 (1984).
8. K. Hasselmann, *et al.*, 'Measurements of wind-wave growth and swell decay during the Joint North Sea Wave Project (JONSWAP)', *Dtsch. Hydrogr. Z. A*, **8**, 1–94 (1973).
9. S. Hasselmann *et al.*, 'Computations and parameterizations of the nonlinear energy transfer in a gravity-wave spectrum. Part II: Parameterizations of the non-linear energy transfer for application in wave models', *J. Phys. Oceanogr.*, **15**, 1378–1391 (1985).
10. N. Booij and L. H. Holthuijsen, 'Propagation of ocean waves in discrete spectral models', *J. Comput. Phys.*, **68**, 307–326 (1987).
11. N. N. Yanenko, *The Method of Fractional Steps*, Springer, 1971.
12. P. J Roache, *Computational Fluid Dynamics*, Hermosa, Albuquerque, NM, 1976.
13. J. C. Chen *et al.*, 'The measurement and analysis of waves under typhoon conditions in the coastal waters of Hong Kong', *Technical Report*, Department of Civil and Structural Engineering, Hong Kong Polytechnic, 1987.
14. C. P. Jelesnianski, 'Numerical computations of storm surges without bottom stress', *Mon. Weather Rev.*, **94**, 379–394 (1966).